Optimization of SLM Process Parameters for Ti6Al4V Medical Implants

El-Sayed, Mahmoud; Ghazy, Mootaz; Yehia, Youssef; Essa, Khamis

DOI:
10.1108/RPJ-05-2018-0112

Optimization of SLM Process Parameters for Ti6Al4V Medical Implants

Abstract

Ti6Al4V alloy has received a great deal of attention in medical applications due to its biomechanical compatibility. However, the human bone stiffness is between 10 and 30 GPa while solid Ti6Al4V is significantly stiffer, which would cause stress shielding with the surrounding bone which can lead to implant and/or the surrounding bone's failure. In this work, the effect of SLM process parameters on the characteristics of Ti6Al4V samples, such as porosity level, surface roughness, elastic modulus and compressive strength (UCS), has been investigated using Response Surface Method (RSM). The examined ranges of process parameters were 35-50 W for laser power, 100-400 mm/s for scan speed and 35-120 μm for hatch spacing. The results showed that the porosity % of a SLM component could be increased by reducing the laser power and/or increasing the scan speed and hatch spacing. It was also shown that there was a reverse relationship between the porosity level and both the modulus of elasticity and UCS of the SLM part. In addition, the increased laser power resulted in a substantial decrease of the surface roughness of SLM parts. The process parameters have been optimized to obtain structures with properties very close to that in human bones. Results from the optimization study revealed that the interaction between laser process parameters (i.e. laser power, laser speed, and the laser spacing) have the most significant influence on the mechanical properties of fabricated samples. The optimized values for the manufacturing of medical implants were 49 W, 400 mm/s and 99 μm for the laser power, laser speed and laser spacing, respectively. The corresponding porosity, surface roughness, modulus of elasticity and UCS were 23.62%, 8.68 μm, 30 GPa and 522 MPa, respectively.

Keywords: Selective laser melting (SLM); Design of Experiment; Ti-6Al-4V; Medical Implants

1. Introduction

Selective laser melting (SLM) is an additive manufacturing technique that produces near fully dense metal parts directly from a CAD design by adding layer upon layer [1-4]. The main concept is based on a laser beam that passes over a thin layer of powder and diffuses it selectively to the desired shape. Next, a new layer of powder is spread, the platform is lowered according to the required layer thickness and then the melting process is repeated until the full part is obtained [5,6]. SLM has many advantages such as producing complex shapes that are difficult to fabricate via conventional methods, short time from design to market, and near net shape production which minimizes waste of materials [7,8]. For these reasons, the SLM process is used in aerospace and biomedical applications such as implants and prostheses [9,10]. Examples of metal powder used in SLM processes are: titanium alloys, steels, cobalt, chromium and aluminum alloys [11]. On the other hand, SLM has some limitations that include the stair step effect which increases surface roughness, and balling phenomenon which increases both the surface roughness and the porosity of SLM parts [12].

The quality of the SLM fabricated parts depends upon many parameters such as the size and morphology of the powder used. Another important factor is the laser heat input as it affects the degree of consolidation of the powder particles as well as the formation of any defects. One of the approaches to represent the laser heat input is the energy density function Ψ, which could be expressed according to equation 1 as follows [13]:

$$\varphi = \frac{P}{vht} \qquad (1)$$

Where P is the laser power, v is the scan speed, h is the hatch spacing and t is the layer thickness. Many researchers [14] applied this function to correlate the density of SLM samples with the heat input, but with a common aim to fabricate fully solid components by identifying an optimum energy density level corresponding to minimum porosity content [15]. On the other hand several studies suggested the use statistical analysis by means of design of experiments (DoE) techniques such as the Response Surface Method, and the Analysis of Variance (ANOVA). One of the most favourite RSM designs is the Central Composite Design (CCD). In this design the number of factors examined is noted as "k". The design is a combination of two-level factorial (known as cube points), face points (also known as axial points) and centre points. The axial points are controlled through a statistical parameter called α. For Central Composite Design, α is larger than one and each factor is varied over 5 levels (- α, -1, 0, 1 and α) [16]. Designs for k = 2 and k = 3 factors are shown in Fig 1 below. These techniques were successfully applied to investigate the influence of process parameters such as laser power, scan speed and scan spacing on the resulting surface quality and porosity content in Selective Laser Sintering (SLS) and SLM processes [17,18].

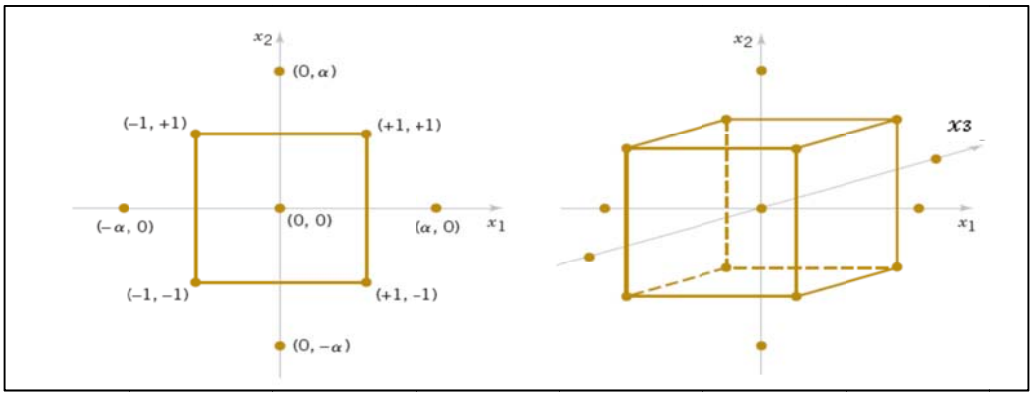

Fig 1. Central composite designs for *k* = 2 and *k* = 3 [**16**].

Attar et al. [19] stated that titanium alloys are very compatible with SLM technique. The microstructure and mechanical properties of parts produced via SLM can be graded in a controlled manner. This makes the technology suitable for biomedical applications in which manufacturing complex shapes of functional implants from biocompatible metals is crucial. Ti6Al4V alloy is among the most commonly used Ti materials for implant applications because of its biocompatible nature [20-22]. It has low density, good mechanical properties, high corrosion resistance and relatively low Young's modulus of approximately 110 GPa. Furthermore, strength, stiffness, corrosion behavior and process accuracy were suitable for medical applications.

Song et al. [23] have studied the effect of the processing parameters on the characteristics of Ti6Al4V SLM parts. They reported that fully-solid Ti6Al4V parts have been successfully manufactured by selective laser melting using the following parameters

(laser power = 110 W, scan speed = 400 mm/s, scan spacing = 40 μm, and layer thickness = 50 μm). Sun et al. [24] used the Taguchi method to optimize four process parameters: layer thickness, linear energy density, hatch spacing and scanning strategy. They reported that 80 W laser power, 200 mm/s scan speed, 60 μm hatch spacing, a 20 μm layer thickness and X-Y inter-layer for scanning strategy was sufficient to achieve fully dense, good quality Ti6Al4V components. In another study Murr et al. [25] have produced Ti6Al4V parts via SLM for biomedical implants. It was indicated that SLM was capable of producing good quality parts with mechanical properties better than wrought and cast Ti6Al4V parts. Vandenbroucke and Kruth [26] also produced medical and dental parts fromTi6Al4V alloy and tested their mechanical and chemical properties. The Ti6Al4V produced had achieved 99.98 % density.

However, it should be noted that in the earlier studies such as those by Murr [25] and Vandenbroucke and Kruth [26], the objective was mainly to produce SLM parts with minimum porosity in order to achieve mechanical properties that could reach, or even exceed, those of bulk material. In the work reported by Vandenbroucke and Kruth [26], a tensile young's modulus of about 94 GPa was obtained. Nevertheless, the elastic modulus of bones in human body ranges from 10 to 30 GPa. The large difference in moduli between titanium implants and bones, known as stiffness mismatch, can result in stress shielding, which has been held responsible for implant loosening and consequently could cause the patients to require a revision surgery. Two solutions were found to this problem: the first one was developing new types of titanium alloys that have modulus closer to bones and the second one was developing porous structure instead of solid structures which reduces material modulus [27-30].Titanium alloys that have 30% volume porosity can have modulus similar to human bones. One problem of porous structures is that it decreases toughness and creates stress concentration around the pores [31].

Furthermore, a medical implant should have high compressive strength to prevent fractures and improve functional stability. High strength is also required to impede spring-back both during and after the operation procedure [32,33]. Finally, an implant should have sufficient surface roughness to improve the ingrowth of the human tissues into it. Compared to smooth surfaces, textured implants surfaces exhibit more surface area for integrating with bone via osseointegration process. It was suggested that a surface roughness in the range from 1 to 10 microns would be required to enhance both the osteoconduction (in-migration of new bone), and osteoinduction (new bone differentiation) processes [34-36].

Previous investigations related to additive manufacturing of Ti alloys have focused on producing fully dense and high integrity structures. There is a clear gap in literature regarding the simultaneous enhancement and adjustment of pore fraction, surface and mechanical properties of Ti6Al4V SLM components towards biomedical implants. In the present work, artificial pores have been created in Ti6Al4V parts fabricated via SLM by controlling the process parameters to achieve surface and mechanical properties suitable for biomedical applications. The influence of processing parameters by means of laser power, scan speed and hatch spacing on the surface roughness, porosity content and mechanical properties of Ti6Al4V components produced by SLM will be investigated. Statistical analysis by means of Design of Experiments (DoE) and Analysis of Variance (ANOVA) will be adopted to optimise the SLM process parameters and fabricate custom parts with elastic modulus, UCS and surface roughness sufficiently close to that of human bones.

2. Experimental Methods

2.1 Materials

Ti6Al4V gas atomized alloy powder was supplied by LPW Technology. Most of the powder particles had a size range between 19-45μm as measured using a laser diffraction analyzer (Microtrac) following the ASTM B822 standard. The size distribution of powder used is shown in Table 1.

Table 1. Ti6Al4V powder size distribution

Particle size (μm)	<16	16-22	22-31	31-44	>45
Percentage (%)	5	10	28	46	11

2.2. Statistical design of experiment (DoE) using response surface

In this study the design of experiment RSM was carried out to generate an experimental plan with minimum possible trials. ANOVA was utilized to find a relationship between the input and output parameters, identify the most significant parameters, and find the optimal setting of those parameters that can achieve the intended objective function. The response surface "Y" can be expressed by a second order polynomial (regression) equation as shown in Equation 2:

$$Y = b_o + \sum b_i x_i + \sum b_{ii} x_i^2 + \sum b_{ij} x_i x_j \qquad (2)$$

where x_i are the factors input parameters. The terms b_0, b_i, b_{ii}, and b_{ij} are the model coefficients that depend on the main and interaction effects of the process parameters. Method of least squares is used to determine the constant coefficients. To perform the design of experiment, Design-Expert Software Version 7.0.0 (Stat-Ease Inc., Minneapolis, USA) was used.

The procedure adopted in this study was as the following:

1. Identification of the key process parameters, and setting the upper and lower bound for each.
2. Selection of the output response.
3. Developing the experimental design matrix.
4. Carrying out the experiments according to the design matrix, and recording the output response.
5. Developing a mathematical model to correlate the process parameters to the output response.
6. Optimizing that model using genetic algorithm.

In the current study three factors (process parameters) were considered which are the laser power, scan speed and hatch spacing. According to the central composite design, and as described above, each parameter was varied over 5 levels (-α, -1, 0, 1 and α). See Fig 1. In this work α was considered to be 2 in order to change each factor over five equal levels. Table 2 shows the levels of each factor in this investigation. As shown -α and α represent the minimum and maximum levels respectively, of each factor. Also, three center points (at the 0 level (middle) of all factors, see Fig1) were considered. The center points are used to provide

information about the experimental error. This resulted in the identification of 17 parametric combinations for testing, as shown in Table 3. Porosity content, surface roughness, elastic modulus and compressive strength (UCS) were measured as outputs to better understand the quality characteristics of the fabricated samples.

2.3. Sample build and characterization

SLM components were fabricated using the SLM system (ProX 100TM) from 3D systems at Texas A&M University, USA. All specimens were built using a Z-increment (vertical) of 30 µm. All processing was carried out in an Argon atmosphere with an oxygen-content of less than 0.1%. A small coupon with rectangular cross-section of 6 mm x 6 mm, and with a height of 12 mm was fabricated for each parametric condition.

Table 2. The range of matrix building parameters.

Parameter	Units	Levels				
		-2	-1	0	1	2
Laser Power	W	35	39	43	46	50
Scan Speed	mm/s	100	175	250	325	400
Hatch Spacing	µm	35	56	78	99	120

The surface roughness of fabricated coupons was measured by surface profilometer (Taylor Hobson Form Talysurf 120L). In this work, the surface quality of the parts was mostly expressed by the arithmetic mean surface roughness (Ra). Four measurements were carried out for each sample, two at the top surface and another two at the side. The Ra was measured over a length of 4 mm. The mean value of these four center-line average surface roughness was considered to express the surface roughness of each sample.

The samples were prepared for microscopic examination using standard mechanical grinding and polishing using SiC paper down to a 0.05 µm finish. Polished surfaces were examined using a Zeiss AxioVert A1 optical microscope equipped with AxioVision 4 image analysis software. Eight frames captured for each sample (each with a size of 800 µm x 600 µm) and the area fraction of the pores was evaluated using ImageJ image analysis software. The compression tests were conducted using a WDW-100E universal testing machine using a constant loading speed of 2 mm/min. The resulting compression test' stress-strain curves were analyzed to obtain the ultimate compressive strength and the elastic modulus for each specimen. Table 3 shows the 17 parametric conditions used in this investigation and the corresponding quality characteristics.

3. Results and Discussion

The measured values for surface roughness, porosity %, elastic modulus and ultimate compressive strength along with the parametric combinations are presented in Table 3.

Table 3. Matrix building parameters with resulting surface roughness, porosity %, elastic modulus and ultimate compressive strength.

Run	Laser Power (W)	Scan Speed (mm/s)	Hatch Spacing (µm)	Surface Roughness (µm)	Porosity %	Elastic Modulus (GPa)	Ultimate Compressive Strength (MPa)
1	46	325	99	10.12	20.03	24.07	492
2	35	250	78	20.34	14.56	31.35	748
3	43	100	78	16.03	5.29	63.91	1631
4	39	325	56	16.99	9.91	46.80	1114
5	39	325	99	17.11	25.43	17.12	388
6	46	175	56	12.41	2.94	74.98	1749
7	46	325	56	12.27	4.39	66.93	1665
8	39	175	56	20.33	2.63	71.58	1501
9	43	250	78	15.15	7.65	54.48	1243
10	43	400	78	14.94	23.09	20.81	467
11	50	250	78	9.10	3.86	66.43	1636
12	43	250	78	14.58	7.80	48.93	1212
13	43	250	120	14.58	21.70	21.63	427
14	39	175	99	16.51	6.18	59.18	1342
15	46	175	99	11.81	3.01	69.64	1540
16	43	250	78	15.11	7.77	53.04	1258
17	43	250	35	13.42	3.57	68.83	1537

3.1. ANOVA results

In statistical analysis, Least square fitting R^2 is used to describe the model fit. RSM method suggested that both surface roughness and modulus of elasticity fit linear models with R^2 of 92% and 87% respectively. Additionally, porosity content fits a quadratic model with R^2 of 98% while UCS fits a two-factor interaction model with R^2 of 95%. The predicted versus actual plots for modulus of elasticity, porosity, surface roughness and UCS are shown in Figs 2 (a) to (d), respectively. The observed points on all plots reveal that the actual values are distributed relatively near to the straight line in all cases. This could suggest that each of the models reasonably described the relationship between the process parameters and the different responses evaluated in this study. The four models can be represented as functions of laser power (P), scan speed (v) and hatch spacing (h) which could be described using the general empirical model (Equation 3).

$$\text{Response} = b_o + b_1(P) + b_2(v) + b_3(h) + b_4(Pv) + b_5(Ph) + b_6(vh) + b_7(P)^2 + b_8(v)^2 + b_9(h)^2 \quad (3)$$

Where b_o is the average response, and b_1, b_2. . .,b_9 are the model coefficients that depend on the main and interaction effects of the process parameters. Least Squares Fitting, which is a mathematical procedure for finding the best-fitting curve to a given set of points by minimizing the sum of the squares of the offsets of the points from the curve, was applied to

analyze the data presented in Table 3 and to determine the constant coefficients. The values of the model coefficients for the four quality characteristics are shown in Table 4.

Table 4.Response surface model coefficients for the surface roughness and porosity fraction.

Coefficient	Surface roughness model	Porosity model	Elastic modulus model	Ultimate compressive strength model
bo	+14.76	+7.17	+50.57	+1173.38
b1	-2.92	-2.20	+6.94	+179.93
b2	-0.42	+5.04	-12.92	-300.16
b3	-0.26	+4.44	-11.54	-280.50
b4	0	-1.01	0	+26.03
b5	0	-0.42	0	-62.18
b6	0	+3.44	0	-191.22
b7	0	+0.30	0	0
b8	0	+1.54	0	0
b9	0	+1.15	0	0

In statistical significance testing the p-value is the probability of obtaining a test statistic at least as extreme as the one that was actually observed, assuming that the null hypothesis is true. The null hypothesis (which assumes that all parameters have no significant effect) is rejected when the p-value is less than the predetermined significance level which is 0.05 (95% confidence level). This means that any factor has p-value less than 0.05 is considered to be a significant model parameter [37]. Table 5 shows the p-value for each parameter and interaction. In this study the ANOVA results indicated that, within the investigated range of parameters, the most significant parameters influencing the surface roughness was the laser power while the modulus of elasticity was mainly affected by laser power, scan speed and hatch spacing. Finally, both the porosity % and UCS were significantly affected by the three process parameters as well as the interaction between scan speed and hatch spacing.

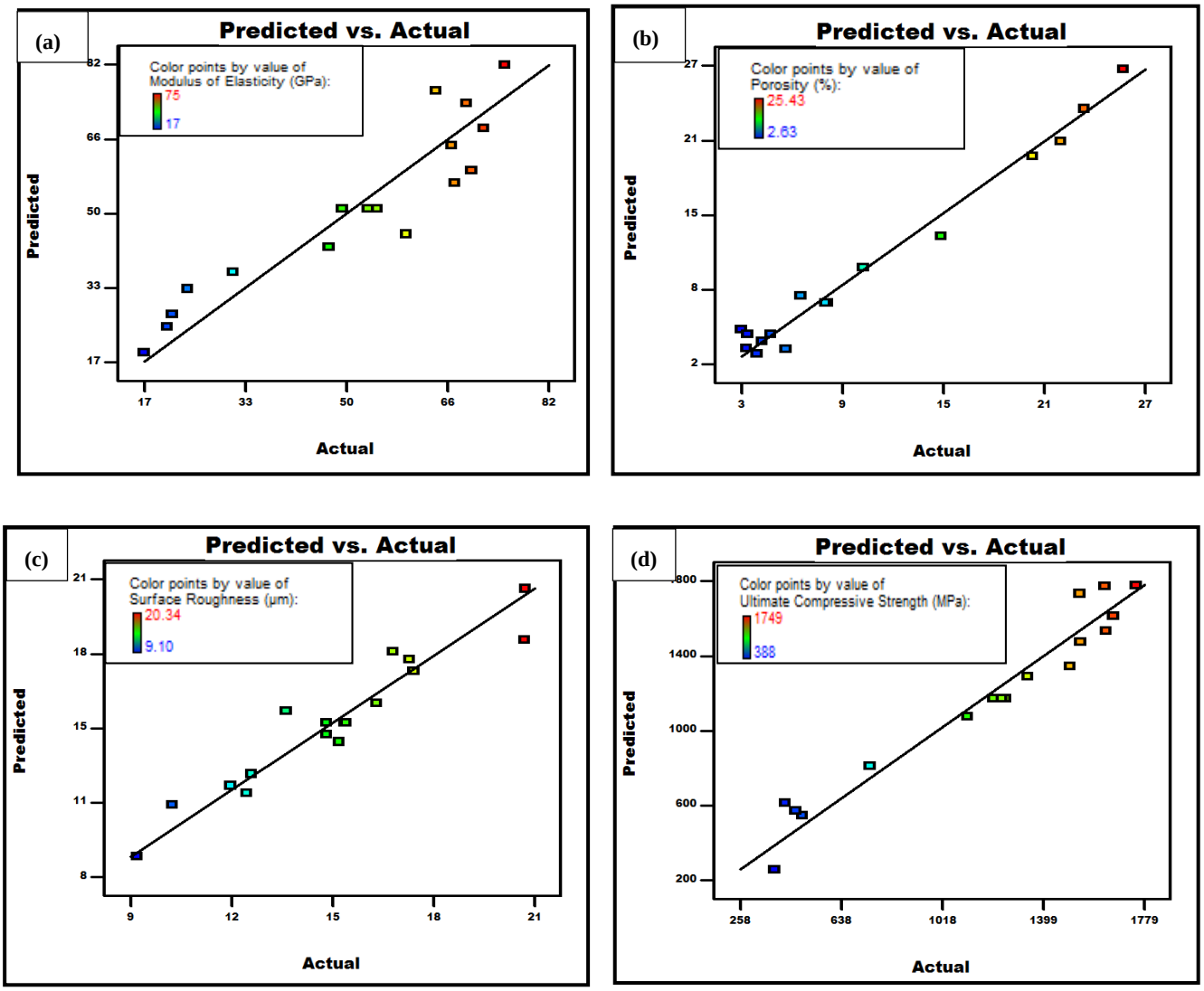

Fig 2. Design-Expert plot. Predicted vs actual data for different properties of SLM part, (a) modulus of elasticity, (b) porosity, (c) surface roughness and (d) UCS.

Table 5.ANOVA p-values for each of the parameters and parameter interactions for the Ra, porosity %, elastic modulus and UCS.

Model Parameter	P-value			
	Surface roughness	Porosity %	Elastic modulus	Ultimate compressive strength
P	**< 0.0001***	**0.0016**	**0.0051**	**0.0004**
V	0.1108	**< 0.0001**	**< 0.0001**	**< 0.0001**
H	0.3144	**< 0.0001**	**< 0.0001**	**< 0.0001**
Pv	N.A.	0.1519	N.A.	0.6030
Ph	N.A.	0.5239	N.A.	0.2285
vh	N.A.	**0.0009**	N.A.	**0.0028**
P^2	N.A.	0.4855	N.A.	N.A.
v^2	N.A.	0.0065	N.A.	N.A.
h^2	N.A.	0.0243	N.A.	N.A.

*Bold values indicate statistically significant process parameters (p-value<0.05)

3.1.1. Surface roughness analysis

As indicated before, only the laser power was found to have a significant effect on the surface roughness and that relationship between them follows a linear model. Fig 3 shows the effect of laser power on surface roughness. It can be seen that increasing the laser power from 35 to 50 W, at constant scan speed and hatch spacing of 250 mm/s and 78 µm respectively, resulted in a significant drop of the R_a value from 21 to 9 µm.

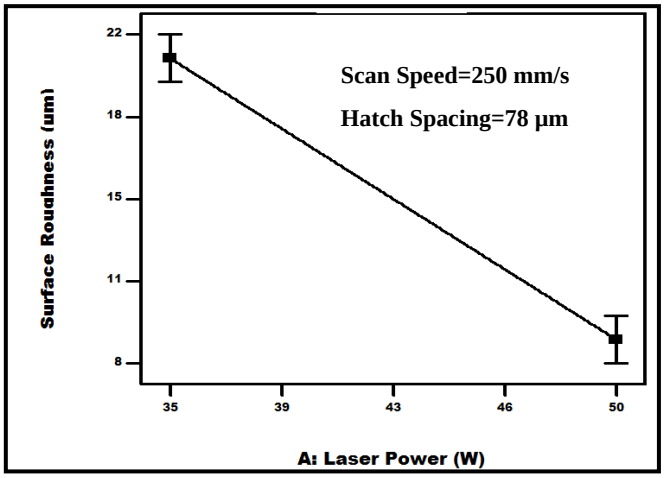

Fig 3. Effect of laser power on the surface roughness.

This suggests that increasing the laser power could significantly reduce the roughness of both top and side surface of the SLM parts. Higher laser power generates large recoil pressures which cause the melt pool to flatten resulting in a better quality of the top surface [38]. In addition, the increased laser power increases the energy density which improves the wettability of the melt pool, eliminating the differences in surface tension and in turn decreasing the chance of encountering the balling phenomenon which dramatically decreases the side surface roughness [2]. In a study by Yasa and Kruth [39], the surface roughness of Ti6Al4V SLM parts fabricated using 40 W laser power, 225 mm/s scan speed and 74 µm hatch spacing (optimized parameters for maximum density) was measured to be 15 µm. In the current study, and as could be inferred from Fig 3, the surface roughness at 40W laser power, 250 mm/s scan speed and 78 µm hatch spacing is about 16.5 µm, which shows good agreement with the result obtained by Yasa and Kruth [40]. Again, for biomedical application, implants with rough surfaces are preferred to allow tissues to grow inside and integrating them to the hosting bones. This can be achieved by using low laser power.

3.1.2. Porosity analysis

Figs 4 (a), (b) and (c) show the effect of laser power, scan speed and hatch spacing on the porosity content using quadratic model as suggested by the RSM. It can be seen that the porosity content in the SLM fabricated coupons decreased consistently with increasing the laser power and/or decreasing the scan speed and hatch spacing. High laser power and/or low scan speed will increase the energy density applied to the powder and improve the diffusion process. Additionally, when high energy is applied, pores are closed under surface tension and capillary forces which increase the density of SLM samples. Also, low scan speed ensures that continuous tracks can be obtained. Small hatching spacing would increase the overlapping area of adjacent scanning lines, resulting in a complete melting of the powder

between scanning lines. In this way, the subsequent melting pool would grow on the solidified scanning lines and the preceding solidified layer, causing the scanning line to proceed stably from melt to solid [41]. Finally, the model suggests that the interaction between the hatch spacing and scan speed is also significant, as shown in Fig 4 (d). At higher hatch spacing the effect of scan speed on porosity formation is more considerable. This phenomenon was also reported by Hassanin and co-workers during the fabrication of Ti6Al4V micro-components using selective laser melting [42].

Figs 4 (e) and (f) show micrographs of samples 15 and 2, respectively (See Table 3). The porosity content of sample 15 and sample 2 was 3.01% and 14.56%, respectively. It could be noticed that when relatively low scan speed and high laser power are used (sample 15), the material was considerably denser (Fig 4 (e)). On the other hand, when high scan speed and low laser power are used, the energy density was not enough to consolidate the powder, which leads to porous structures (Fig 4 (f)). In biomedical applications, a Ti implant with structure similar to that in sample 2 is recommended as it has low elastic modulus. Additionally, the pores will help tissues to easily grow and integrate with the implant.

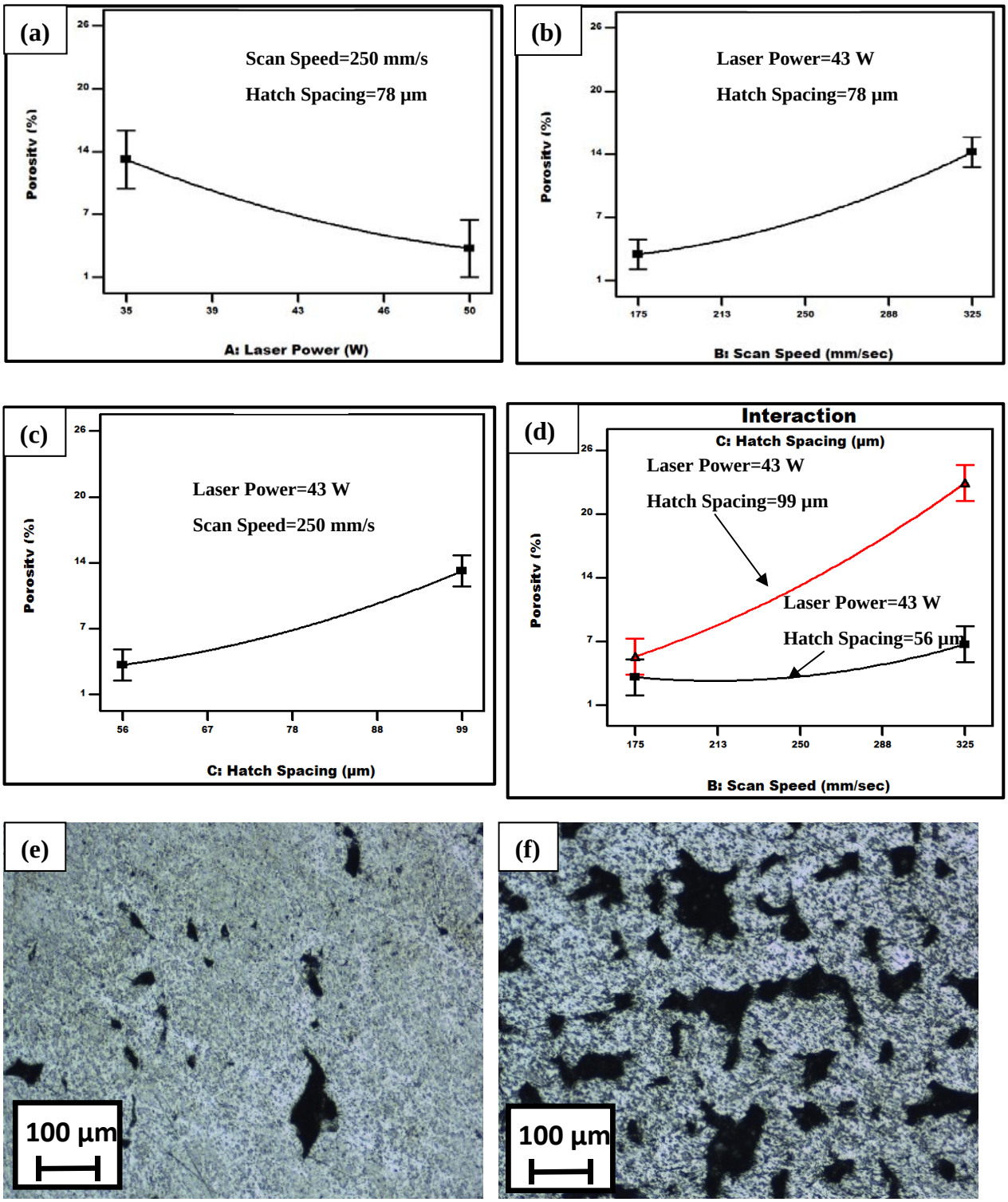

Fig 4. Effect of (a) laser power, (b) scan speed, (c) hatch spacing and (d) the interaction between speed and hatch spacing on the porosity; (e) and (f) are micrographs of samples 15 and 2 respectively.

3.1.3. Analysis of Elastic modulus

All the three process parameters were found to have significant effect on the elastic modulus of fabricated samples as shown in Figs 5. Elastic modulus was found to be a linear function of the three parameters. The modulus of elasticity was shown to increase by increasing the laser power, as shown in Fig 5 (a). The same effect on properties could be

achieved by decreasing the scan speed and/or the hatch spacing, as could be inferred from Figs 5 (b) and (c) respectively.

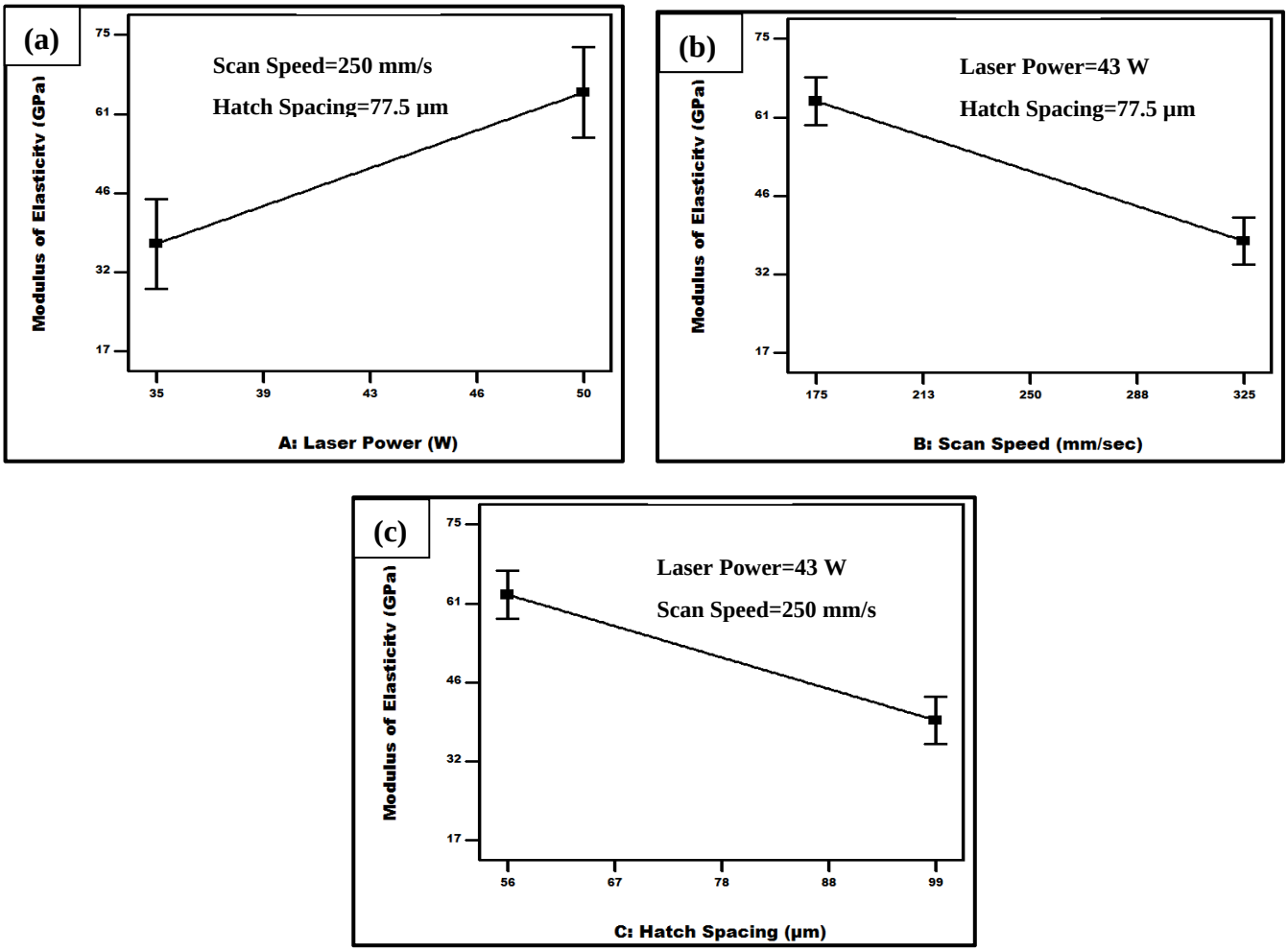

Fig 5. Effect of (a) laser power, (b) scan speed and (c) hatch spacing on the elastic modulus.

3.1.4. Analysis of UCS

Similar to the elastic modulus, the UCS was suggested by the model to have a direct relationship with the laser power and reverse relationship with both the scan speed the hatch spacing (See Figs 6 (a), (b) and (c)). In addition, the interaction between scan speed and hatch spacing was found also to significantly affect the UCS. At the same laser power, increasing the hatch spacing resulted in a steeper slop of the relationship between the scan speed and the UCS, as seen in Fig 6 (d). However, UCS was suggested to be represented as a two-factor interaction (2FI) model of the SLM process parameters.

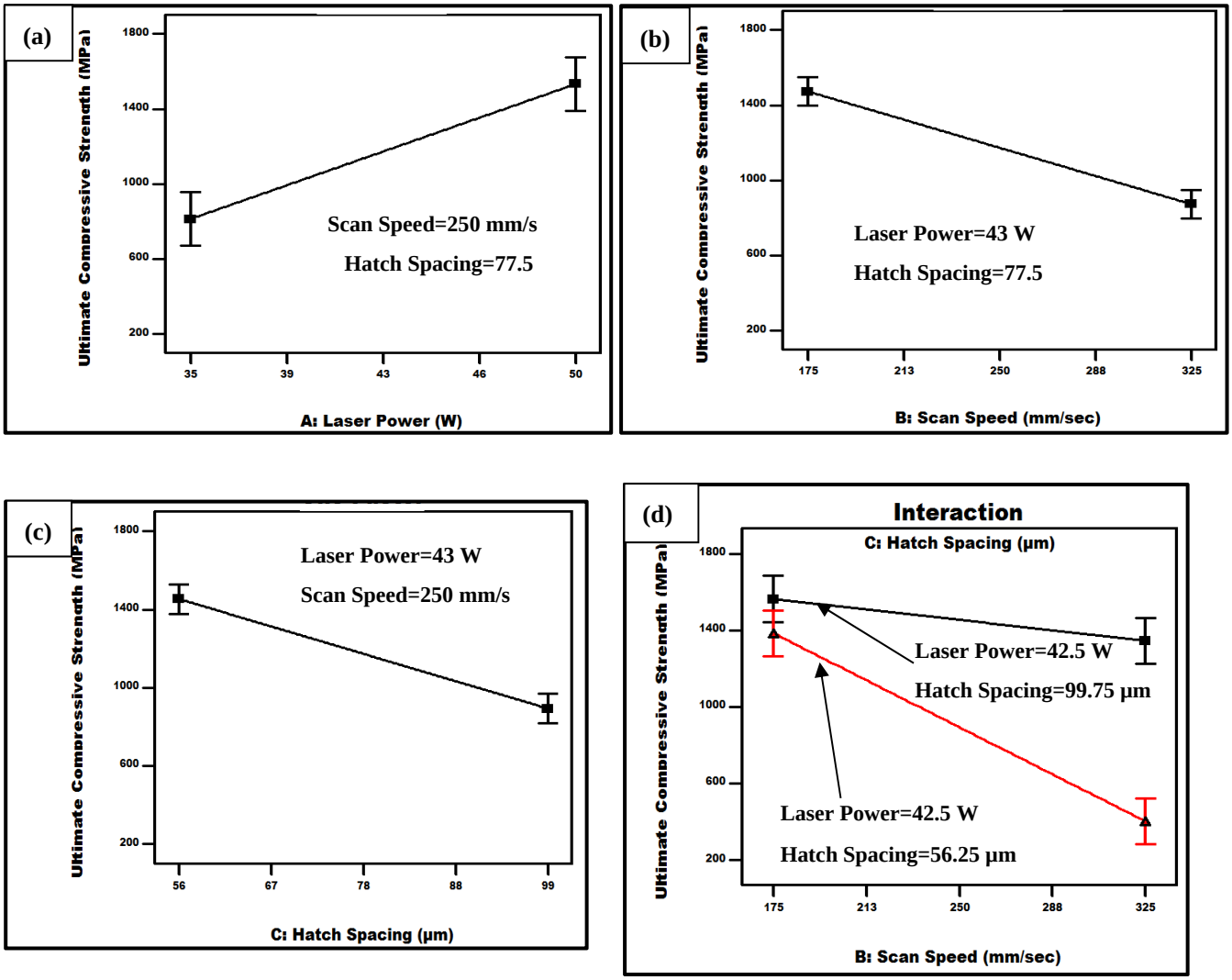

Fig 6. Effect of (a) laser power, (b) scan speed, (c) hatch spacing and (d) the interaction between speed and hatch spacing on the UCS.

From the results presented in Table 3 and those shown in Figs 4 to 6, it could be indicated that a strong correlation was shown between the results of the porosity % and both the elastic modulus and UCS results. It has been suggested that the porosity is known to significantly control the mechanical properties [43]. This could be easily shown by comparing samples number 5 and 6 of the parametric combinations shown in Table 3. Decreasing the porosity % from 25.43 to 2.94 resulted in a significant increase in the elastic modulus from 17 to 75 GPa, and a comparable rise in the UCS from 388 to 1749 MPa.

3.4. Rationalizing the porosity formation using the energy density

Fig 7 (a) shows a plot of porosity versus the energy density form the data shown in Table 3. It should be noted that unless the energy density is sufficient to melt and diffuse the powder, the final build would end with pores as a result of the incomplete melting. Increasing the scan speed and hatch spacing and/or a decrease in the laser power shall reduce the melt pool and lead to incomplete consolidation. This would result in entrapment of the voids among the powder particles under the solidified hatch lines, increasing the porosity content and in turn reducing the overall density of the SLM part (See also Fig 4) which is an important requirement for Ti implants. As shown in Fig 7 (a), the porosity content consistently decreases with increasing the energy density, which is expected due to the

improved consolidation of the metal powder, until achieving a minimum value at a range of energy density from 90 to 130 J/mm^3. However, further increase of the energy density causes the porosity content to scatter beyond that level until 180 J/mm^3. In this region, other defects such as keyhole formation (due to vaporization) might be produced within the SLM part, which increases the overall porosity level. The presence of a threshold for the energy density that gives maximum density of Ti6Al4V SLM parts was reported in earlier studies to be in the range of 100 to 120 J/mm^3 [27,42].

In addition, the change of both the elastics modulus and UCS of SLM parts with the porosity % are presented in Figs 7 (b) and (c), respectively. It is obvious that both the elastic modulus and UCS correlate well with the porosity %, which confirmed the results of previous studies [43]. Also, it was shown that at relatively low porosity levels (2-3%), both the elastic moulds and UCS were fairly high, reaching values of 75 GPa and 1800 MPa, respectively, achieving the performance of a solid material. The elastic modulus and UCS of solid Ti6Al4V are 119 GPa and 1080 MPa, respectively [44]. Obtaining UCS of SLM parts that are higher than that of the solid material was reported by other researchers during the study of mechanical behavior of commercially pure Ti [19], and Ti6Al7Nb alloys [45]. The achievement of mechanical properties of Ti6Al4V SLM parts that were superior to those of the bulk material was also reported by Song et al. [15] and Vandenbroucke and Kruth [46].

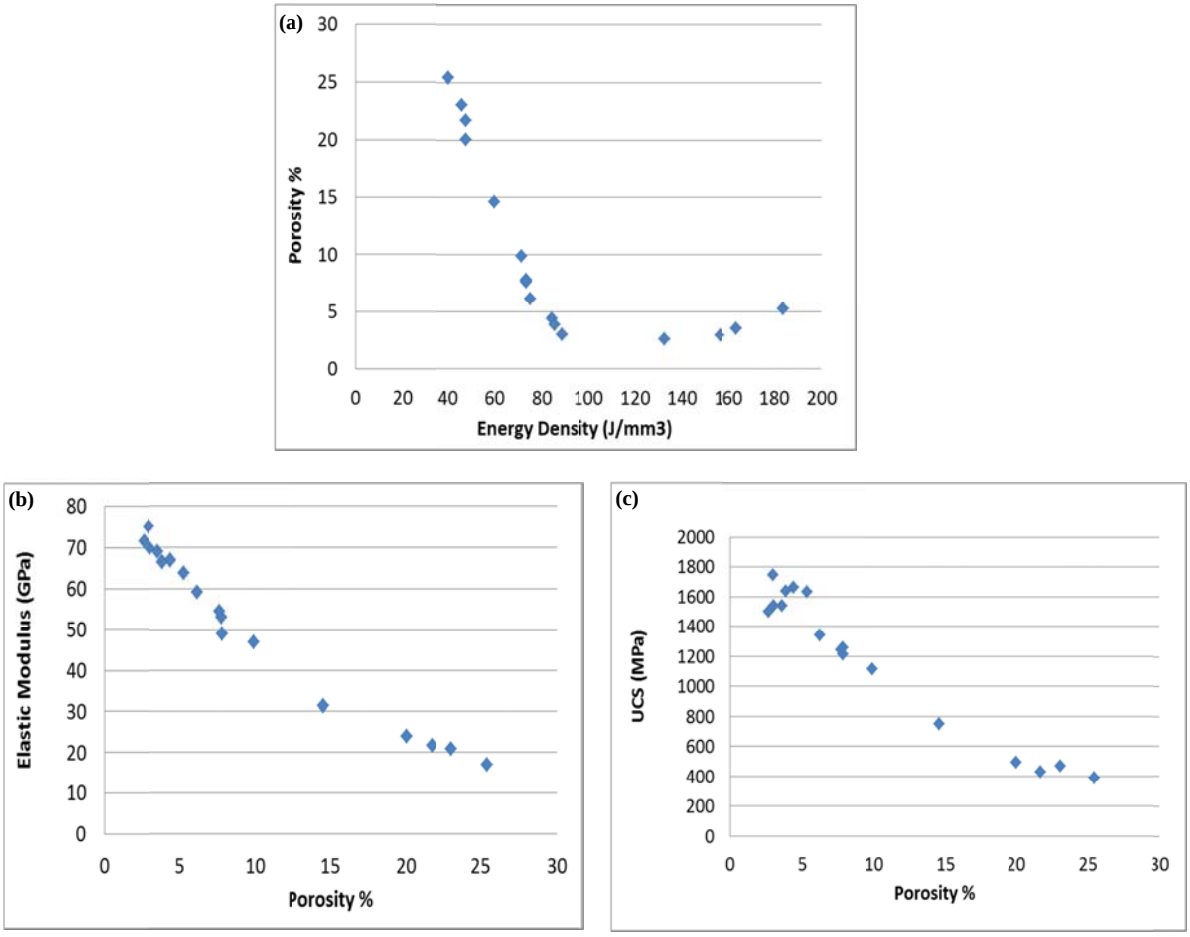

Fig 7. (a) Porosity variation versus the energy density, (b) and (c) variation of elastic modulus and UCS with porosity %, respectively.

3.5. Optimization towards medical applications

Titanium alloys, particularly Ti6Al4V, are among the most commonly used materials in the medical and dental industries because of their superior biocompatibility, corrosion

resistance and specific strength [47]. Despite their attractive properties, some Ti6Al4V implants suffer an instability during service due to stress shielding and the weak interfacial bond between the insert and the surrounding tissues [48]. The elastic modulus of Ti6Al4V is around 119 GPa while it is ranging from 10 to 30 GPa for human bone and henceforth parts produced using Ti6Al4V have considerably higher stiffness than natural bone [49]. Such stiffness mismatch is recognized as one reason of stress shielding of the bone. Stress shielding prevents the needed stress being transferred from the implant to adjacent bone, which might result in bone loss in the near-vicinity of implants. The usage of porous structures is one of the approaches used to overcome this problem. The materials in this case possesses significantly lower elastic modulus and hence lower stiffness when compared to a the dense one [50]. Likewise, a permeable insert gives a fabulous organic environment to the body fluid or medication to transport productively through the porosity. Therefore, the encompassing tissues can grow inside the implant and consequently improve its interfacial bonding with natural bone [51]. Also, and described above, a microtopographic profile of an implant with a surface roughness in the range from 1-10 μm would be appropriate to improve the osteoconducstion through variations in surface topography, and osteoinduction along the implant surface by employing the implant as a carrier for local transport of bio active agents such as bone morphogenic Protein [35]. However; relatively higher surface roughness may result in an increase in ionic leakage as well as peri-implantilis [36]. Again high compressive strength of an implant is essential for better endurance against service conditions[32].

Therefore, an optimization study has been carried out to explore the optimum setting of processing parameters necessary to SLM of a Ti6Al4V component with characteristics suitable for orthopaedic surgery. The objective function was set to obtain an elastic modulus in the range from 10 to 30 GPa, and a surface roughness between 1 and 10 micron while achieving the highest corresponding UCS and porosity %. The experimental data was analyzed by the Design-Expert software and the genetic algorithm was used to predict the process parameters that satisfy the objective function. The response equations describing the porosity, surface roughness, elastic modulus and UCS in terms of the key process parameters (shown in Equation (3) and the related coefficients listed in Table 4) were solved simultaneously.

The prediction results given in Fig 8 show the contour plot for the optimization function of elastic modulus, porosity, surface roughness and UCS, for a range of laser power (35-50 W) and scan speed (100-400 mm/s). The model suggests that the optimized values of the process parameters would be 49 W laser power, 400 mm/s scan speed and 99 μm hatch spacing. This is equivalent to an energy density of 45 J/mm^3. At these values of process parameters; the predicted modulus of elasticity, porosity, surface roughness and UCS of a SLM part would be 30 GPa, 23.62%, 8.68 μm, and 522 MPa, respectively.

Several researchers have reported the use of SLM for controlling porosity during fabrication of Ti6Al4V medical implants [43,52,53]. Their results showed that creating pores in a Ti6Al4V part had a significant role in reducing its stiffness, which could allow the implant to have an elastic modulus that is close to that of human cortical bone. During the manufacturing of Ti6Al4V open-porous scaffolds using SLM, Weißmann and co-authors [43] concluded that a structure with a porosity % between 43 and 80 experienced an elastic modulus in the range from 26.3 to 3.4 GPa and an UCS in the range from 750 to 100 MPa. In the current study it was predicted that at 23.62% porosity the elastics modulus and UCS of the SLM part would be 30 GPa and 522 MPa, respectively. Such variation might be attributed

to the fact that in the current work a solid part containing a certain amount of porosity was produced while in the study by Weißmann lattice structures were fabricated. In another study by Oh et al. [54], porous titanium compacts were prepared by powder sintering. The results of this study showed that a Ti part with a porosity level of about 28% had an elastic modulus of about 30 GPa which was too close to the model prediction in the current study.

It should be emphasized that the obtained results are only valid within the examined process window. Outside that window, other phenomena, such as melt pool turbulence or evaporation, might take place. This shall affect the characteristics of melt pool, which could influence the formation of porosity, hence affects the mechanical properties.

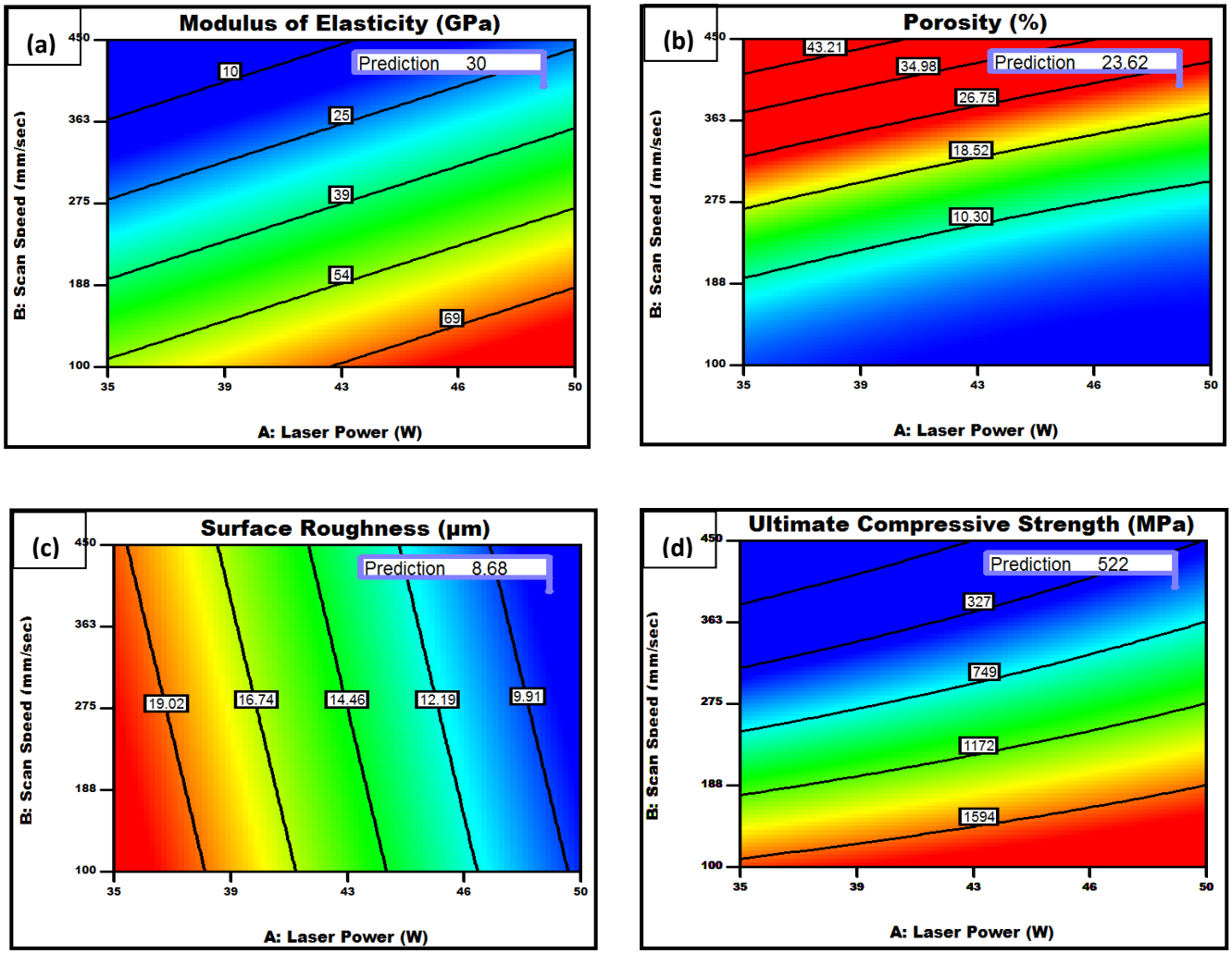

Fig 8. Predicted optimum laser power and scan speed (at a hatch spacing of 90 µm) for desirable properties of a SLM part suitable for medical implants; (a)elastic modulus (10-30 GPa), (b) maximum porosity %, (c)surface roughness (1-10 µm) and (d) highest UCS.

3.6. Model Validation

To examine the results predicted by the model, 3 identical Ti6Al4Vparts with a square cross-section of 6x6 mm and with a height of 12 mm were SLM fabricated using the optimum setting of process parameters i.e. 49 W laser power, 400 mm/s scan speed and 99 µm hatch spacing using the same layer thickness of 30 µm. The samples are shown in Fig 9. Table 6 shows the measured values of the properties of the three samples. As shown, the average values of the modulus of elasticity, porosity %, surface roughness and UCS of the three samples were 27.14 GPa, 24.90, 9.55 µm and 509 MPa, respectively.

Fig 9. SLM coupons fabricated using the optimized process parameters

Table 6. Elastic modulus, porosity%, surface roughness and UCS of the three samples produced using optimized process parameters.

Sample	Elastic Modulus (GPa)	Porosity %	Surface Roughness (μm)	Ultimate Compressive Strength (MPa)
1	30.33	24.74	9.63	512
2	26.20	25.10	9.43	487
3	24.89	24.86	9.59	527
Av.	27.14	24.90	9.55	509

Figs 10 (a), (b) and (c) show a micrograph, an experimental stress-strain diagram and the measured surface roughness profile of the side surface, respectively, of a sample number 2 of the three samples produced using the optimized process parameters.

From the results of the 17 experiments carried out during the DoE, shown in Table 3, the lowest elastic modulus was 17.12 GPa and the corresponding surface roughness was 17.11 μm. On the other hand, the lowest surface roughness was found to be 9.1 μm and the corresponding elastic modulus was 66.43 GPa, which is too difficult to be used for medical implants. The results of the process optimisation showed that the predicted optimum elastic modulus that could be achieved within the investigated process window was 30, which is suitable for medical applications. In addition, the corresponding surface roughness was 9.55 μm, which also falls within the range suitable for medical implants.

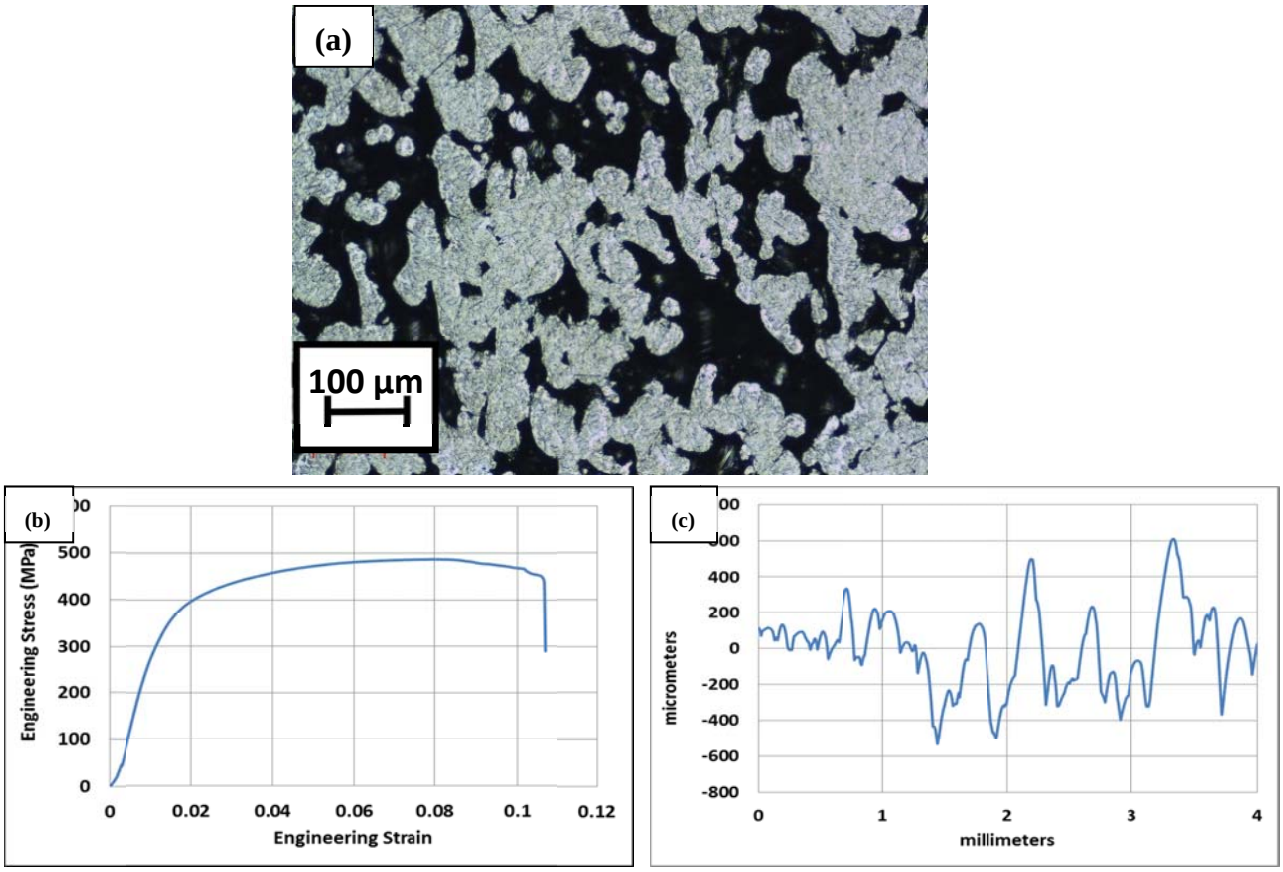

Fig 10. (a) An optical microscope image, (b) A fracture compression test results and (c)A typical surface roughness profile of a SLM sample produced using optimized conditions for a medical implant.

4. Conclusions

The influence of the SLM process parameters on the quality characteristics of Ti6Al4V SLM parts, by means of elastic modulus, porosity content surface roughness and UCS, was investigated. Response Surface Method and Analysis of Variance were used to generate an experimental plan and identify the most significant parameters. The generic algorithm was used to find the optimal setting of process parameters that can produce parts with properties suitable for orthopaedic structure. Based on the obtained results, the following points can be concluded;

1. Increasing the laser power was found to significantly reduce the surface roughness of the SLM component, most probably due to the associated flattening of the melt pool, which decreases the top roughness, and the elimination of the balling phenomenon which is expected to enhance the quality of the side surfaces of SLM parts.

2. Increasing the laser power and/or decreasing the scan speed and hatch spacing (within a certain range) resulted in a reduction of the porosity level of the SLM part, because of the improved consolidation of the metallic powder) and accordingly the modulus of elasticity and UCS of the part were increased. In addition, the mechanical properties of a SLM component correlated well with the pore fraction indicating a possibility for tailoring the properties via a carful control of the porosity level of a SLM part.

3. Setting the process parameters at 49 W laser power, 400 mm/s scan speed and 99 μm hatch spacing was found to be optimum and resulted in SLM parts with 23.62%, porosity level, 8.68 μm surface roughness, 30 GPa modulus of elasticity and 522 MPa UCS. These properties were suggested to be suitable for orthopaedic structure with stiffness close to that in human bones, and also to improve the bone in-growth characteristics.

Acknowledgment

The authors would like to thank Dr. Alaa Elwany from the Department of Industrial & Systems Engineering at Texas A&M University in USA for his great help and support in producing the samples using his SLM system (ProX 100TM).

References

1. Essa K, Modica F, Imbaby M, El-Sayed MA, ElShaer A, Jiang K, Hassanin H (2017) Manufacturing of metallic micro-components using hybrid soft lithography and micro-electrical discharge machining. Int J Adv Manuf Technol 91 (1-4):445-452

2. Kruth JP, Froyen L, Van Vaerenbergh J, Mercelis P, Rombouts M, Lauwers B (2004) Selective laser melting of iron-based powder. Journal of Materials Processing Technology 149 (1–3):616-622. doi:http://dx.doi.org/10.1016/j.jmatprotec.2003.11.051

3. Mumtaz K, Hopkinson N (2009) Top surface and side roughness of Inconel 625 parts processed using selective laser melting. Rapid Prototyping Journal 15 (2):96-103. doi:doi:10.1108/13552540910943397

4. Essa K, Sabouri A, Butt H, Basuny FH, Ghazy M, El-Sayed MA (2018) Laser additive manufacturing of 3D meshes for optical applications. PloS one 13 (2):e0192389

5. Yadroitsev I, Bertrand P, Smurov I (2007) Parametric analysis of the selective laser melting process. 253:8064-8069. doi:10.1016/j.apsusc.2007.02.088

6. Li S, Hassanin H, Attallah MM, Adkins NJ, Essa K (2016) The development of TiNi-based negative Poisson's ratio structure using selective laser melting. Acta Materialia 105:75-83

7. Thijs L, Verhaeghe F, Craeghs T, Humbeeck JV, Kruth J-p (2010) A study of the microstructural evolution during selective laser melting of Ti – 6Al – 4V. Acta Materialia 58 (9):3303-3312. doi:10.1016/j.actamat.2010.02.004

8. Sabouri A, Yetisen AK, Sadigzade R, Hassanin H, Essa K, Butt H (2017) Three-dimensional microstructured lattices for oil sensing. Energy & Fuels 31 (3):2524-2529

9. Chlebus E, Kurzynowski T, Dyba B (2011) Microstructure and mechanical behaviour of Ti — 6Al — 7Nb alloy produced by selective laser melting. 62:3-10. doi:10.1016/j.matchar.2011.03.006

10. Yadroitsev I, Smurov I (2011) Surface Morphology in Selective Laser Melting of Metal Powders. 12:264-270. doi:10.1016/j.phpro.2011.03.034

11. Kumar S, Pityana S Laser-based additive manufacturing of metals. In: Advanced Materials Research, 2011. Trans Tech Publ, pp 92-95

12. Strano G, Hao L, Everson RM, Evans KE (2013) Surface roughness analysis , modelling and prediction in selective laser melting. Journal of Materials Processing Tech 213 (4):589-597. doi:10.1016/j.jmatprotec.2012.11.011
13. Read N, Wang W, Essa K, Attallah MM (2015) Selective laser melting of AlSi10Mg alloy : Process optimisation and mechanical properties development. Materials and Design 65:417-424. doi:10.1016/j.matdes.2014.09.044
14. Olakanmi EO, Cochrane RF, Dalgarno KW (2011) Densification mechanism and microstructural evolution in selective laser sintering of Al–12Si powders. Journal of Materials Processing Technology 211 (1):113-121. doi:http://dx.doi.org/10.1016/j.jmatprotec.2010.09.003
15. Song B, Dong S, Zhang B, Liao H, Coddet C (2012) Effects of processing parameters on microstructure and mechanical property of selective laser melted Ti6Al4V. Materials & Design 35:120-125. doi:http://dx.doi.org/10.1016/j.matdes.2011.09.051
16. El-Sayed MA (2018) Parametric analysis of SLM process for fabricating 316L stainless steel samples by response surface method.
17. Bacchewar PB, Singhal SK, Pandey PM (2007) Statistical modelling and optimization of surface roughness in the selective laser sintering process. Proceedings of the Institution of Mechanical Engineers, Part B: Journal of Engineering Manufacture 221 (1):35-52. doi:10.1243/09544054jem670
18. Carter LN (2013) Selective laser melting of nickel superalloys for high temperature applications. University of Birmingham, Birmingham
19. Attar H, Calin M, Zhang L, Scudino S, Eckert J (2014) Manufacture by selective laser melting and mechanical behavior of commercially pure titanium. Materials Science and Engineering: A 593:170-177
20. Vaithilingam J, Prina E, Goodridge RD, Hague RJ, Edmondson S, Rose FR, Christie SD (2016) Surface chemistry of Ti6Al4V components fabricated using selective laser melting for biomedical applications. Materials Science and Engineering: C 67:294-303
21. Dai N, Zhang L-C, Zhang J, Chen Q, Wu M (2016) Corrosion behavior of selective laser melted Ti-6Al-4V alloy in NaCl solution. Corrosion Science 102:484-489
22. Dai N, Zhang J, Chen Y, Zhang L-C (2017) Heat Treatment Degrading the Corrosion Resistance of Selective Laser Melted Ti-6Al-4V Alloy. Journal of The Electrochemical Society 164 (7):C428-C434
23. Song B, Dong S, Zhang B, Liao H, Coddet C (2012) Effects of processing parameters on microstructure and mechanical property of selective laser melted Ti6Al4V. Materials and Design 35:120-125. doi:10.1016/j.matdes.2011.09.051
24. Sun J, Yang Y, Wang D (2013) Parametric optimization of selective laser melting for forming Ti6Al4V samples by Taguchi method. Optics and Laser Technology 49:118-124. doi:10.1016/j.optlastec.2012.12.002
25. Murr LE, Quinones SA, Gaytan SM, Lopez MI, Rodela A, Martinez EY, Hernandez DH, Martinez E, Medina F, Wicker RB (2009) Microstructure and mechanical behavior of Ti – 6Al – 4V produced by rapid-layer manufacturing , for biomedical applications. 2 (1):20-32. doi:10.1016/j.jmbbm.2008.05.004
26. Ben Vandenbroucke J-PK (2006) SELECTIVE LASER MELTING OF BIOCOMPATIBLE METALS FOR RAPID.148-159

27. Zhang LC, Attar H (2016) Selective laser melting of titanium alloys and titanium matrix composites for biomedical applications: a review. Advanced Engineering Materials 18 (4):463-475
28. Liu Y, Li X, Zhang LC, Sercombe T (2015) Processing and properties of topologically optimised biomedical Ti–24Nb–4Zr–8Sn scaffolds manufactured by selective laser melting. Materials Science and Engineering: A 642:268-278
29. Liu Y, Li S, Wang H, Hou W, Hao Y, Yang R, Sercombe T, Zhang LC (2016) Microstructure, defects and mechanical behavior of beta-type titanium porous structures manufactured by electron beam melting and selective laser melting. Acta Materialia 113:56-67
30. Hassanin H, Al-Kinani AA, ElShaer A, Polycarpou E, El-Sayed MA, Essa K (2017) Stainless steel with tailored porosity using canister-free hot isostatic pressing for improved osseointegration implants. Journal of Materials Chemistry B 5 (47):9384-9394
31. Nasr S, Taheri M, Shayesteh N (2016) Independent tuning of stiffness and toughness of additively manufactured titanium-polymer composites : Simulation , fabrication , and experimental studies. Journal of Materials Processing Tech 238:22-29. doi:10.1016/j.jmatprotec.2016.06.035
32. Saini M, Singh Y, Arora P, Arora V, Jain K (2015) Implant biomaterials: A comprehensive review. World Journal of Clinical Cases: WJCC 3 (1):52
33. Yan L, Yuan Y, Ouyang L, Li H, Mirzasadeghi A, Li L (2016) Improved mechanical properties of the new Ti-15Ta-xZr alloys fabricated by selective laser melting for biomedical application. Journal of Alloys and Compounds 688:156-162
34. Stanford C (2008) Surface modifications of dental implants. Australian dental journal 53 (s1)
35. Alla RK, Ginjupalli K, Upadhya N, Shammas M, Ravi RK, Sekhar R (2011) Surface roughness of implants: a review. Trends in Biomaterials and Artificial Organs 25 (3):112-118
36. Le Guéhennec L, Soueidan A, Layrolle P, Amouriq Y (2007) Surface treatments of titanium dental implants for rapid osseointegration. Dental materials 23 (7):844-854
37. Carter LN, Essa K, Attallah MM (2015) Optimisation of selective laser melting for a high temperature Ni-superalloy. Rapid Prototyping Journal 21 (4):423-432
38. Morgan R, Sutcliffe CJ, O'Neill W (2004) Density analysis of direct metal laser re-melted 316L stainless steel cubic primitives. Journal of Materials Science 39 (4):1195-1205. doi:10.1023/B:JMSC.0000013875.62536.fa
39. Yasa E, Deckers J, Kruth JP (2011) The investigation of the influence of laser re-melting on density, surface quality and microstructure of selective laser melting parts. Rapid Prototyping Journal 17 (5):312-327. doi:10.1108/13552541111156450
40. Yasa E, Kruth J-P (2011) Microstructural investigation of Selective Laser Melting 316L stainless steel parts exposed to laser re-melting. Procedia Engineering 19:389-395
41. Sun J, Yang Y, Wang D (2013) Parametric optimization of selective laser melting for forming Ti6Al4V samples by Taguchi method. Optics & Laser Technology 49:118-124. doi:http://dx.doi.org/10.1016/j.optlastec.2012.12.002

42. Hassanin H, Modica F, El-Sayed MA, Liu J, Essa K (2016) Manufacturing of Ti–6Al–4V Micro-Implantable Parts Using Hybrid Selective Laser Melting and Micro-Electrical Discharge Machining. Advanced Engineering Materials 18 (9):1544-1549
43. Weißmann V, Wieding J, Hansmann H, Laufer N, Wolf A, Bader R (2016) Specific Yielding of Selective Laser-Melted Ti6Al4V Open-Porous Scaffolds as a Function of Unit Cell Design and Dimensions. Metals 6 (7):166
44. Boyer R, Welsch G, Collings EW (1994) Materials Properties Handbook: Titanium Alloys. ASM International, Materials Park, OH,
45. Chlebus E, Kuźnicka B, Kurzynowski T, Dybała B (2011) Microstructure and mechanical behaviour of Ti—6Al—7Nb alloy produced by selective laser melting. Materials Characterization 62 (5):488-495
46. Vandenbroucke B, Kruth J-P (2007) Selective laser melting of biocompatible metals for rapid manufacturing of medical parts. Rapid Prototyping Journal 13 (4):196-203
47. Kurgan N (2014) Effect of porosity and density on the mechanical and microstructural properties of sintered 316L stainless steel implant materials. Materials & Design 55:235-241. doi:http://dx.doi.org/10.1016/j.matdes.2013.09.058
48. Dewidar MM, Khalil KA, Lim JK (2007) Processing and mechanical properties of porous 316L stainless steel for biomedical applications. Transactions of Nonferrous Metals Society of China 17 (3):468-473. doi:http://dx.doi.org/10.1016/S1003-6326(07)60117-4
49. Bender S, Chalivendra V, Rahbar N, El Wakil S (2012) Mechanical characterization and modeling of graded porous stainless steel specimens for possible bone implant applications. International Journal of Engineering Science 53:67-73. doi:http://dx.doi.org/10.1016/j.ijengsci.2012.01.004
50. Bandyopadhyay A, Espana F, Balla VK, Bose S, Ohgami Y, Davies NM (2010) Influence of porosity on mechanical properties and in vivo response of Ti6Al4V implants. Acta Biomaterialia 6 (4):1640-1648. doi:http://dx.doi.org/10.1016/j.actbio.2009.11.011
51. Wiria FE, Shyan JYM, Lim PN, Wen FGC, Yeo JF, Cao T (2010) Printing of Titanium implant prototype. Materials & Design 31, Supplement 1:S101-S105. doi:http://dx.doi.org/10.1016/j.matdes.2009.12.050
52. Mullen L, Stamp RC, Brooks WK, Jones E, Sutcliffe CJ (2009) Selective Laser Melting: A regular unit cell approach for the manufacture of porous, titanium, bone in-growth constructs, suitable for orthopedic applications. Journal of Biomedical Materials Research Part B: Applied Biomaterials 89 (2):325-334
53. Van Bael S, Kerckhofs G, Moesen M, Pyka G, Schrooten J, Kruth J-P (2011) Micro-CT-based improvement of geometrical and mechanical controllability of selective laser melted Ti6Al4V porous structures. Materials Science and Engineering: A 528 (24):7423-7431
54. Oh I-H, Nomura N, Masahashi N, Hanada S (2003) Mechanical properties of porous titanium compacts prepared by powder sintering. Scripta Materialia 49 (12):1197-1202